Modelling and Analysis of Frequency-Responsive Wind Turbine Involved in Power System Ultra-Low Frequency Oscillation

Li Sun, *Member, IEEE,* Xiaowei Zhao

***Abstract*—This paper presents a dynamic analysis for ultra-low frequency oscillations (ultra-LFOs) observed in the wind-hydropower hybrid systems. In such systems, DFIG wind turbines (WTs) are required to be frequency-responsive with providing the inertia and frequency support. First, this paper establishes an analytical model to capture the dynamics of frequency-responsive DFIG WTs at the electromechanical timescale. A systematic analysis is then conducted on a 2-machine system (include a hydraulic generator (HG) and an aggregated DFIG WT) to reveal WTs' dynamic behaviors and their interference mechanism with the HG, accounting for the system ultra-LFO mode. The result shows that WTs' frequency control, speed control, MPPT control and pitch control would be involved in the system ultra-LFOs, but they have different effects under different operating modes. Cases studies are carried out on the 2-machine system and a modified 10 machine 39-bus New-England power system. Based on the modelling effort and simulation studies, some recommendations are made for using DFIG WTs to help damp the ultra-LFO in wind-hydropower hybrid systems.**

***Index Terms*—DFIG wind turbine, hydraulic generator, inertia and damping support, proportional & derivative (PD)-frequency control, ultra-low frequency oscillation (LFO).**

NOMENCLATURE

$L_s/x_s,\ L_m/x_m$	Stator and mutual inductance/inductive impedance
$\omega_0,\ \omega$	Unit/real value of synchronous speed
$\omega_r,\ \omega_{slip}$	Electrical angular/slip speed of wind turbine rotor
$P_w,\ H_r$	Mechanical power and equivalent mechanical inertia
$P,\ Q$	Electrical active and reactive power
$\boldsymbol{E},\ \boldsymbol{V}, \boldsymbol{I}$	Internal voltage, terminal voltage and current vectors
$E,\ V,\ I$	Magnitude of $\boldsymbol{E},\ \boldsymbol{V},\ \boldsymbol{I}$
$k_{p\omega},\ k_{i\omega}$	PI parameters of speed control
$k_{p\beta 1},\ k_{p\beta},\ k_{i\beta}$	Parameters of pitch control
$ref,\ 0,\ \Delta$	Reference, steady-state, perturbational value
$s,\ r$	Stator, rotor-side variables

I. INTRODUCTION

The ultra-low frequency oscillation (ultra-LFO) problems have been observed in the hydropower dominant power systems, such as Hydro-Quebec system [1], Colombian power grid [2] and Yunnan Power Grid in the South China [3], etc. They have different mode frequencies and causes, compared to inter-area LFOs. Inter-area LFOs (with a mode frequency at around 0.1 1Hz) are characterized by one or more units in one region oscillating against one or more units located in another region, typically geographically distant in a power grid [2]. Such LFOs likely appear when two groups of generation units are weakly connected through tie lines. Basically, inter-area LFOs are mostly related to rotor angle oscillations and caused by inter-machine interactions. In contrary, ultra-LFOs have a lower oscillation frequency (around 0.05Hz) and they are usually doomed to be the consequence of unstable frequency/governor control and water hammer phenomenon [2], [4]. They always cause a wide-area problem since they could easily propagate over a very small line impedance in the grid. One most intuitive and appealing countermeasure of such ultra-LFO problems is to tune the governor control parameters and hence to create an enhanced damping at the ultra-LFO mode [3], [5].

In recent years, the wind-hydropower hybrid systems become prevailing, like Hydro-Quebec system [6], with a rapidly growing penetration of wind power in power systems. Wind turbines (WTs) would be involved in the ultra-LFOs under some circumstances and their control flexibility might provide some potential mitigation solutions. To the best knowledge of authors, this paper is first to provide a systematic analysis on the ultra-LFO problems in WTs connected hydropower-dominant systems.

A WT consists of a mechanical system, electrical system and control system. The low-frequency modes (in the range $<$ 2Hz [7]) of the mechanical system and turbine control exist but are always hidden by the fast-action electrical and control system. That is to say, WTs are less sensible to and hardly make any contribution to damping the ultra-LFO mode in the power systems. However, with the growing integration of wind power, power systems have been drastically suffering from a low system inertia and insufficient dynamic frequency support. In order to deal with this problem, wind power has been invoked to provisionally stabilize the power system with additional frequency control, as stipulated in grid codes in many countries [8], [9]. The additional frequency control (including inertia and primary frequency control) allows WTs to spontaneously help rebalance the power system during load perturbations by releasing/absorbing the kinetic energy stored in WTs' mechanical components. In this way, the mechanical components and their slow controls are coupled to the power systems. While they are able to contribute to resisting the system frequency excursion, a physical path is shed leading to their dynamic interference with the power systems. Such dynamic interference tends to provoke WTs' mechanical components involved in the low-frequency oscillations (like ultra-LFOs) in power systems.

Thus, frequency-responsive WTs (that are fitted with addi-

This work was funded by the UK Engineering and Physical Sciences Research Council under grant EP/S001905/1.

L. Sun and X. Zhao (corresponding author) are with the Intelligent Control & Smart Energy (ICSE) Research Group, School of Engineering, University of Warwick, Coventry, CV4 7AL, U.K. (e-mail: Li.Sun.1@warwick.ac.uk; xiaowei.zhao@warwick.ac.uk).

tional frequency control) have a considerable participation in determining the ultra-LFO stability in the wind-hydropower hybrid systems. However, additional frequency control is designed by complying with the stiff frequency regulation requirement to ensure a sufficient frequency/power support against load perturbations, which is not at all responsible for damping the ultra-LFOs during the course of design. In this sense, frequency-responsive WTs may provide a negative damping and thus pose a threat of the ultra-LFO instability under some circumstances. It would be profound to reveal the underlying mechanism of frequency-responsive WTs involved in the ultra-LFO problem.

There are some papers associated to stability issues of WTs connected power systems. The reported models and achievements are primarily direct at conventional LFO problems [10], [11], dynamic frequency stability [12], [13] and subsynchronous oscillation problems [14], [15]. Based on time-scale separation and singular perturbations, the cause and effect analysis in [10]–[15] are carried out by capturing the corresponding dynamics of the mechanical and converter control system. However, (i) the ultra-LFO problem is not covered in these cited papers, and (ii) the reported models are not available for the ultra-LFO problem due to the absence of the control with a response bandwidth lower than 0.1Hz [16], [17] (like MPPT and pitch angle control). Reference [18] has investigated the ultra-LFO problems in WTs connected systems. In [18], a particle-swarm-optimization (PSO)-based inertia control is proposed for WTs to help mitigate the ultra-LFOs. However, it is not mentioned that the impact mechanism of control and operating mode of WT itself on the ultra-LFOs. The WTs' impact is but should not be underestimated for highly wind penetrated power systems. Readers are referred to Table V in Appendix for more information.

Having in mind that (i) WTs' output power is drastically impacted by the rotor speed and aerodynamic power; and that (ii) actions of the MPPT and pitch angle control vary with the operation mode. Thus, it is crucial to model the dynamic power characteristics along the whole operating trajectory for the ultra-LFO problem in wind-hydropower systems. The developed model should (i) include the frequency control, speed control, MPPT control and pitch angle control; and (ii) enable to conduct a systematic analysis on WTs involved in the ultra-LFO issue, by considering different operating modes.

With the aim to fill in the research gap in the ultra-LFO analysis, this paper first makes some improvements on the modelling of WTs in several ways. In contrast to [10]–[15], the speed control and aerodynamics model related to the MPPT and pitch control action are built against different operation modes. The frequency control that consists of inertia and droop frequency control is also captured. Along with the rotor swing equation and the coupling between the system frequency and WT's output power, we finally establish a WT's analytical model for the ultra-LFO analysis. Notably, the analytical model differs from the reported model in [20]. (i) It captures the MPPT action difference under different operating modes; and (ii) it is presented in a symbolic transfer function form, with the frequency perturbation ($\Delta\omega$) as the input and the active power correction (ΔP) as the output. The analytical model allows us to generalize the torque analysis method to reveal the insight into the impact principle of frequency-responsive WTs on the ultra-LFO mode (that appears in the wind-hydropower hybrid systems). On this basis, the novelty and contributions of this paper are outlined here.

- An analytical model of frequency-responsive WTs is developed, by raising awareness on different behaviors of MPPT and pitch control under different operation modes. The model is used for the ultra-LFO analysis, and the damping calculation.
- The impact mechanism of frequency-responsive WTs on the ultra-LFO is evaluated. Following the calculation of the ultra-LFO damping from WTs, it presents a physical insight into the impacts of WTs' control actions and operating modes on the ultra-LFO problem. The analysis results provide guidance for improving the ultra-LFO damping by modifying some controls and reshaping WTs' dynamic behaviors.

Therefore, this paper accommodates an intuitive explanation on the behaviors of frequency-responsive WTs participating in the power system ultra-LFOs, and provides the guidelines for damping the ultra-LFOs using DFIG WTs. The remainder of this paper is organized as follows. Section II introduces a small parametric (2-machine) test system, where a hydraulic generator (HG), an aggregated DFIG WT and a local load are included. In Section III, the WT's analytical model available for the ultra-LFO analysis is established. Section IV is devoted to examining the behaviors of frequency-responsive WTs impacting on the ultra-LFO stability. Section V provides a more rigorous simulation test (using a modified 10-machine 39-bus system) to validate the analytical results. The conclusions are finally drawn in Section VI.

II. Fundamentals for the ultra-LFO study

A. Description of Ultra-LFOs

The power system stability issues have different types of oscillatory modes depending on the involved equipment components and controls. According to the response speed/bandwidth, the system oscillatory mode would have a frequency from several kHz to tens of mHz [22] (as shown in Fig. 1). In this context, the ultra-LFO issue is concerned. It has a lower mode frequency (around 0.05Hz) than the conventional LFO ($0.1 \sim 2.5$Hz). Unlike the conventional LFO that is caused by inter-machine interactions, a critical ultra-LFO appears due to an unstable frequency control process of generators (thus, there is no any energy exchange between rotating masses in the case of ultra-LFOs).

B. 2-Machine Wind-Hydropower Hybrid System

In this context, we introduce a simple wind-hydropower hybrid system (see Fig. 2) for the ultra-LFO analysis. Fig. 3 depicts the control system of the HG and WT. The governor control and turbine model of HG is taken in [21]. The governor has a dynamic slower than 1Hz. A complete DFIG WT model includes the aerodynamics, turbine and generator dynamics, rotor-side converter (RSC), grid-side converter (GSC), and

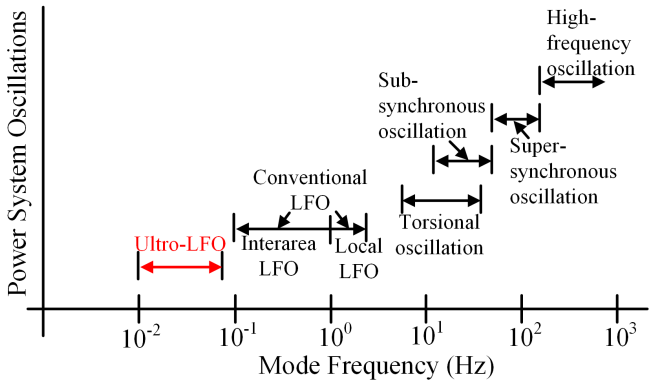

Figure 1. Power system oscillation issues with different mode frequencies.

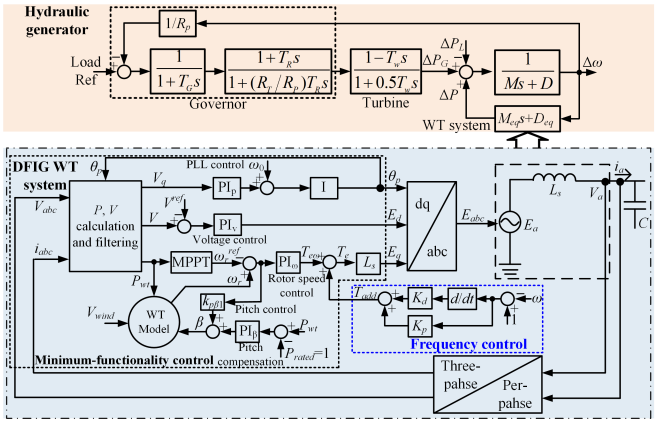

Figure 3. Control block diagram of the 2-machine test system.

DC-link dynamics. In addition, it is fitted with a minimum-functionality control (to capture wind energy and convert to electrical power) and additional frequency control (to enhance the system inertia) [17]. The noteworthy thing is that the WT has a rapid response of DC-link, GSC and its control, with a bandwidth typically larger than 10Hz. The rapid response could be discarded in the course of the ultra-LFO study.

As depicted in Fig. 3, the frequency control usually takes the system frequency as the input and produces a power correction on the original power reference (namely, proportional& derivative (PD)-frequency control in the sequel). It empowers DFIG WTs to be frequency-responsive with the ability of the inertia/frequency support. K_d and K_p are the user-defined inertia constant and damping coefficient, respectively. Note that the PD-frequency control makes DFIG WTs' mechanical dynamics exposed to the external power system. That is, the multi-loop minimum-functionality control would be involved in WTs' frequency behaviours, causing the properties of the inertia and damping from DFIG WT much more complicated. Notably, in the top plot, DFIG WT is modeled by its analytical model. It is produced by forming the input-output ($\Delta\omega$-ΔP) relationship and control blocks (see the bottom plot) in a mathematical way. The details will be given in Section III.

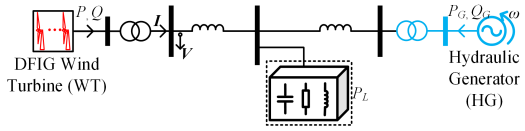

Figure 2. A wind-hydropower hybrid system.

III. Method for Impact Mechanism Analysis of Ultra-LFOs

In a conventional hydropower dominant system, the ultra-LFO is attributed to the mechanical power oscillation that is caused by a negative damping originated from the governor control [3], [5]. This is obtained through the torque analysis method that has been one most straightforward and popular way to conduct the ultra-LFO analysis [23], [24]. By identifying the damping properties, one can readily characterize the nature of the ultra-LFO mode and quantitatively examine the adverse effect of governor control. The results accordingly define the directions of optimizing the governor control [24].

The torque analysis method is then lent for the ultra-LFO study in a wind-hydropower hybrid system (see Fig. 2). To this end, it is crucial to establish an analytical model for the DFIG WT while still preserving its original dynamical properties (to be detailed in the next section). Reference [11] has proposed a thorough modelling for a PMSG WT participating in the power system frequency regulation. A very similar approach can be used to model a frequency-responsive DFIG WT for inertia estimation [12], [13]. As the $-\frac{\Delta P}{s\Delta\omega}$ of WTs is a transfer function but not a scalar (see Fig. 3 in [12]), it means that ΔP has two components in which the one is in proportional to $s\Delta\omega$ and the other one is in proportional to $\Delta\omega$. In analogous to [13], the inertia (M_{eq}) and damping coefficient (D_{eq}) can be both defined to characterize the relationship between ΔP and $s\Delta\omega$, $\Delta\omega$ for WTs. This can be written as $-\frac{\Delta P}{\Delta\omega} = M_{eq}s + D_{eq}$ (as shown in the top part of Fig. 3). Notably, M_{eq} and D_{eq} could be shaped by modifying the frequency control implementation, and they are both zero when no frequency control engages.

In Fig. 2, the swing equation of the common mode frequency oscillation can be approximately described in per unit manner as

$$(M + M_{eq})s\Delta\omega + (D + D_{eq})\Delta\omega = \Delta P_G - \Delta P_L \qquad (1)$$

where $M(= 2H)$ and D are the inertia constant and damping coefficient of the HG, respectively; ω is the average system frequency; P_G is the mechanical power from the hydraulic turbine; P $(= -(M_{eq}s + D_{eq})\omega)$ is the active-power delivery from the interconnected WT; M_{eq} and D_{eq} are the equivalent inertia and damping coefficient of the WT; P_L is the total active component of loads. Note that M_{eq} and D_{eq} can enhance the system inertia and damping, respectively.

In Fig. 3, we have the relationship between ΔP_L and $\Delta\omega$

$$\begin{aligned} -\frac{\Delta P_L}{\Delta\omega} &= (M + M_{eq})s + (D + D_{eq}) \\ &\quad + \frac{1}{R_p}\frac{(1 + T_R s)(1 - T_w s)}{(1 + T_G s)(1 + T_h s)(1 + 0.5T_w s)} \end{aligned} \qquad (2)$$

where $T_h = (R_T/R_p)T_R$. When focusing on the ultra-LFO

mode (with a mode frequency at ω_d), (2) is rewritten as

$$-\frac{\Delta P_L}{\Delta\omega} = (M + M_{eq} + M_G)s + (D + D_{eq} + D_G) \quad (3)$$

associated to the notations

$$\begin{aligned} M_G &= \frac{10M' + T_w^2 M'\omega_d^2 - 3T_w D'}{(4 + T_w^2\omega_d^2)} \\ D_G &= \frac{-2D' - (-T_w D' + M')T_w\omega_d^2}{(4 + T_w^2\omega_d^2)} \\ M' &= \frac{2}{R_p}\frac{(T_G + T_h) + T_R(T_G T_h\omega_d^2 - 1)}{(T_G T_h\omega_d^2 - 1)^2 + (T_G + T_h)^2\omega_d^2} \\ D' &= -\frac{2}{R_p}\frac{[T_R(T_G + T_h) - T_G T_h]\omega_d^2 + 1}{(T_G T_h\omega_d^2 - 1)^2 + (T_G + T_h)^2\omega_d^2} \end{aligned} \quad (4)$$

Given the parameters of the HG ($R_p = 0.05$, $T_G = 0.2$, $T_w = 1$, $T_R = 1$, $R_T = 0.5$, $M = 2H = 12$ and $D = 0$). The HG has a critical ultra-LFO mode at the frequency of 0.06Hz. Then, $M' > 0$ but $D' < 0$ with these values. Thus, M_G is kept positive; D_G is positive for a small ω_d but becomes negative with the increase of ω_d (due to the presence of the water hammer coefficient T_w). In practice, a positive $(D+D_{eq}+D_G)$ is needed to conserve the stability of the ultra-LFO mode. Obviously, there are two improvement ways to this end. One is to increase the the inertia $(M + M_{eq} + M_G)$ to keep the ultra-LFO mode in the low frequency range where a positive D_G could be ensured (referred to [21]). The other one is to fabricate extra damping to increase $(D + D_{eq} + D_G)$. These two ways can be achieved through optimizing HG's governor control [5], [24] or reshaping the value of M_{eq} and D_{eq} of DFIG WT (as explained in Section IV). Thanks to the high controllability and flexibility, it is conceivable to be the most straightforward and appealing to reshape WT's M_{eq} and D_{eq} to resolve ultra-LFOs in wind-hydropower hybrid systems.

Therefore, the torque analysis method can be well generalized to the ultra-LFO analysis on a wind-hydropower hybrid system. In the following section, we establish an analytical model of WTs tailored for the ultra-LFO analysis, based on which we calculate M_{eq} and D_{eq}.

IV. Analytical Model of DFIG WTs

This section is engaged to building the analytical model of DFIG WTs. The dynamic model is first visited by considering the aerodynamics and generator dynamics, the electromechanical control, and the electrical power equations. Using the linearized method, WT's dynamic model is manipulated to form the analytical model. Notably, this analytical model consists of different control actions under different operating modes.

A. Dynamic Model of DFIG WTs

When the dynamics around 0.05 Hz are concerned, the PLL, terminal voltage and inner current control in the DFIG WT are fast enough to be considered reaching the equilibrium state at all times. Hence, the DFIG WT can be modeled by taking into account the aerodynamics and generator model, pitch control, MPPT and speed control, as well as the additional PD-frequency control.

1) Aerodynamics and generator model: The aerodynamics power captured by the WT is expressed as [17]

$$P_w = 0.5\rho C_p(\lambda,\beta)A_r V_w^3,\ \lambda = \omega_r R/V_w \quad (5)$$

where ρ is the air density; A_r is the blade sweep area; R is WT's rotor radius (m); V_w is the wind speed (m/s). $C_p(\lambda,\beta)$ is the power coefficient of the blade which is a function of the pitch angle β and the tip speed ratio λ.

A single rotating mass is used to represent WT's mechanical components. It has a swing equation expressed as

$$P_w - P = 2H_r s\omega_r \quad (6)$$

2) Control model: Fig. 3 depicts the general configuration of a WT control system. A PI control is used to achieve the rotor speed tracking. The speed control is also the active power control due to the use of a one-to-one correspondence between them. The torque/power command $(T_{e\omega})$ from the speed control is obtained

$$T_{e\omega} = (k_{p\omega} + k_{i\omega}/s)(\omega_r - \omega_r^{ref}) \quad (7)$$

The speed reference ω_r^{ref} tracks changes in power output through a MPPT block and a low-pass filter. According to [25], it admits the behavior of MPPT expressed as

$$(1 + T_p s)\omega_r^{ref} = \begin{cases} -0.67P^2 + 1.42P + 0.51 & P_0 < 1 \\ 1.2 & P_0 = 1 \end{cases} \quad (8)$$

where T_p is the filter time constant.

The pitch control consists of a P-type ω_r-regulated control and a PI-type compensation control. Note that the pitch control is deactivated under $P_0 < 1$pu (viz., a below rated-power output) but activated under $P_0 = 1$pu (viz., a rated-power output). Thus, the relation between the pitch angle β and the rotor speed ω_r can be described by

$$(1 + T_\beta s)\beta = \begin{cases} 0 & P_0 < 1 \\ k_{p\beta 1}(\omega_r - 1.2) + G_\beta(P - 1) & P_0 = 1 \end{cases} \quad (9)$$

where $G_\beta = k_{p\beta} + k_{i\beta}/s$; T_β is the filter time constant for pitch control (T_β is set as 0.1 [25] and omitted hereafter). (8) and (9) show that the dynamic behaviors of a DFIG WT vary with its operation mode.

The frequency control couples the power output from a DFIG WT and the system frequency. That is,

$$T_{add} = -(K_d s + K_p)(\omega - \omega_0) \quad (10)$$

where T_{add} represents the power/torque correction originated from the frequency control.

3) Electrical power model: The power output of the DFIG WT comes from the stator and the GSC. Assuming (i) the active power (P_g) of GSC equals to the rotor power when neglecting the loss (hence it equals to the slip power from the stator); and (ii) the reactive power (Q_g) of GSC is generally controlled to be zero. This promises:

$$P_g = -\omega_{slip}P_s = -\omega_{slip}(V_d i_{sd} + V_q i_{sq}),\ Q_g = 0 \quad (11)$$

Under the terminal voltage orientation condition, $V_d = 1$ pu and $V_q = 0$. Then, the total current injection of the WT is

$$\begin{aligned} i_d &= i_{sd} + P_g/V_d = i_{sd} - \omega_{slip}P_s = (1 - \omega_{slip})i_{sd} \\ i_q &= i_{sq} - Q_g/V_d = i_{sq} \end{aligned} \quad (12)$$

Following [13], the relation between the synthetic internal voltage ($\boldsymbol{E}$) and the terminal voltage ($\boldsymbol{V}$) is

$$\boldsymbol{E} = \boldsymbol{V} + jx_s\boldsymbol{I}_s = jx_m\boldsymbol{I}_r \tag{13}$$

where $x_s = \omega_0 L_s$ and $x_m = \omega_0 L_m$. With (11), the equation (12) can be transformed as

$$\begin{aligned} E_d &= -x_m i_{rq} = V_d - x_s i_q \\ E_q &= x_m i_{rd} = V_q + x_s i_d/(1-\omega_{slip}) \end{aligned} \tag{14}$$

in the dq-frame. Therein, $\omega_{slip} = 1 - \omega_r$ is the slip of DFIG.

Equation (14) dictates that a DFIG WT has a similar circuit model as a synchronous generator, while the equivalent reactance is asymmetrical and associated with rotor slip. With (14), the expression of DFIG WT's power output is

$$\begin{aligned} P &= V_d i_d + V_q i_q \\ &= (V_d/x_s)(1-\omega_{slip})(E_q - V_q) - (V_q/x_s)(E_d - V_d) \\ &= (V_d E_q - V_q E_d)/x_s - \omega_{slip}(V_d/x_s)(E_q - V_q) \end{aligned} \tag{15}$$

B. Linearized Model of DFIG WT

When the terminal voltage orientation applied, $V_d = 1$ pu and $V_q = 0$. Then (15) becomes

$$P = \omega_r E_q / x_s \tag{16}$$

The linearization of (16) is obtained

$$\Delta P = (\omega_{r0}/x_s)\Delta E_q + (i_{d0}/\omega_{r0})\Delta\omega_r \tag{17}$$

since $E_{q0}/x_s = i_{d0}/\omega_{r0}$ following the linearization of (14). Combining the perturbed equations of (7), (10) and (14) gives

$$\begin{aligned} \Delta E_q = x_m \Delta i_{rd} = x_s(k_{p\omega} + k_{i\omega}/s)(-\Delta\omega_r^{ref} + \Delta\omega_r) \\ - x_s(K_d s + K_p)\Delta\omega \end{aligned} \tag{18}$$

associated to $i_{rd} = T_{e\omega} + T_{add}$. Linearizing (6) and (8) yields

$$\Delta\omega_r^{ref} = \begin{cases} \frac{h_1}{1+T_p s} & P_0 < 1 \\ 0 & P_0 = 1 \end{cases} \tag{19}$$

where $h_1 = -1.34P_0 + 1.42$. And

$$\Delta P_w - \Delta P = 2H_r\omega_{r0} s \Delta\omega_r \tag{20}$$

In addition, manipulating the linearization of (5) and (9) yields

$$\Delta P_w = \begin{cases} K_1\Delta\omega_r & P_0 < 1 \\ (K_1 + K_2 k_{p\beta 1})\Delta\omega_r + K_2 G_\beta \Delta P & P_0 = 1 \end{cases} \tag{21}$$

where $K_1 = \partial P/\partial\omega_r$ and $K_2 = \partial P/\partial\beta$ at a given operating point. Based on (17)-(21), we establish the linearized DFIG WT model with the following representation (see Fig. 4).

C. Analytical Model of DFIG WT

Depending on the wind condition, the DFIG WT has two different representations of its linearized model, as shown in Fig. 4. This is because that (i) the rotor speed reference ω_r^{ref} is created in different ways and (ii) the pitch control has different actions under the below rated-power operation ($P_0 < 1$pu) and the rated-power operation ($P_0 = 1$pu). Thus, it is nontrivial to explore the analytical mode of DFIG WTs under these two scenarios (Scenario A-$P_0 < 1$pu and Scenario B-$P_0 = 1$pu).

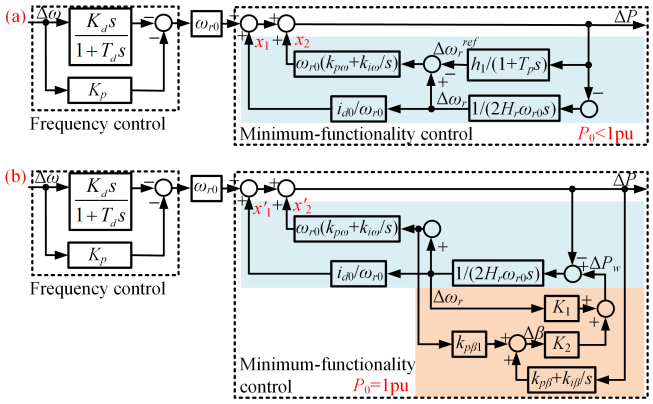

Figure 4. Linearized DFIG WT model: (a) for $P_0 < 1$pu, (b) for $P_0 = 1$pu.

1) Scenario A-$P_0 < 1$pu: In this case, the pitch control is disactivated ($\Delta\beta = 0$); meanwhile, $K_1 = \partial P/\partial\omega_r = 0$ at the steady-state operating point. For convenience, x_1 and x_2 in Fig. 4 (a) (or x_1' and x_2' in Fig. 4 (b)) are used. First, we have

$$\begin{aligned} x_1 + x_2 &= (i_{d0}/\omega_{r0})\,\Delta\omega_r + \omega_{r0}\,(k_{p\omega} + k_{i\omega}/s)\,(\Delta\omega_r - \Delta\omega_r^{ref}) \\ &= (i_{d0}/\omega_{r0} + \omega_{r0}\,(k_{p\omega} + k_{i\omega}/s))\,\Delta\omega_r \\ &\quad - \omega_{r0}\,(k_{p\omega} + k_{i\omega}/s)\,\Delta\omega_r^{ref} \end{aligned} \tag{22}$$

Thus, the system in Fig. 4(a) is accordingly reconstructed and given in Fig. 5. Thus, the open-loop transfer function of

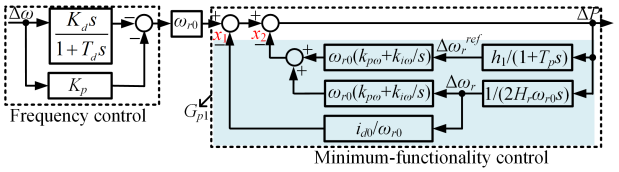

Figure 5. Analytical model of DFIG WTs when $P_0 < 1$pu.

the minimum-functionality control (see the shaded area in Fig. 5) becomes

$$G_{p1} = \omega_{r0}\left(k_{p\omega} + \frac{k_{i\omega}}{s}\right)\frac{h_1}{1+T_p s} + \left(a_2 + \frac{b_2}{s}\right)\frac{1}{s} \tag{23}$$

where $a_2 = \frac{k_{p\omega}}{2H_r} + \frac{i_{d0}}{2H_r\omega_{r0}^2}$, $b_2 = \frac{k_{i\omega}}{2H_r}$. The relationship between ΔP and $\Delta\omega$ is accordingly obtained

$$-\frac{\Delta P}{\Delta\omega} = (K_d s + K_p)\frac{1}{1+G_{p1}} \tag{24}$$

2) Scenario B-$P_0 = 1$pu: The pitch control is activated during the rated-power operation. In this case, the rotor speed reference is cast as constant at its maximum value (i.e., $\omega_r^{ref} = 1.2$pu and $\Delta\omega_r^{ref} = 0$). K_1 and K_2 are both negative and they ensure a positive ΔP_w under the case of $\Delta\omega_r < 0$ and $\Delta\beta < 0$. In Fig. 4(b), the following equation is obtained

$$x_1' + x_2' = (i_{d0}/\omega_{r0})\,\Delta\omega_r + \omega_{r0}\,(k_{p\omega} + k_{i\omega}/s)\,\Delta\omega_r \tag{25}$$

$$\begin{aligned} \Delta P_w = K_1\Delta\omega_r + K_2\Delta\beta = K_1\Delta\omega_r + K_2 k_{p\beta 1}\Delta\omega_r + \\ K_2\,(k_{p\beta} + k_{i\beta}/s)\,\Delta P \end{aligned} \tag{26}$$

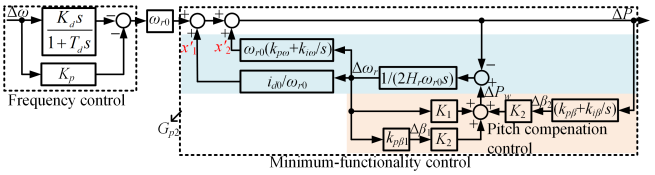

Figure 6. Analytical model of DFIG WTs when $P_0 = 1$pu.

On this basis, the linearized DFIG WT model in Fig. 4(b) is then reconstructed to be the model in Fig. 6.

The concerned open-loop transfer function becomes

$$G_{p2} = \left(a_2 + \frac{b_2}{s}\right) \frac{k'_{p\beta} + k'_{i\beta}/s}{2H_r\omega_{r0}(s + k'_{p\beta 1})} \tag{27}$$

where $k'_{p\beta 1} = \frac{-(K_1+K_2k_{p\beta 1})}{2H_r\omega_{r0}}$, $k'_{p\beta} = 1 - K_2k_{p\beta}$, $k'_{i\beta} = -K_2k_{i\beta}$. Likewise, the relationship of ΔP and $\Delta\omega$ in Fig. 6 can be written as

$$-\frac{\Delta P}{\Delta\omega} = (K_d s + K_p)\frac{1}{1 + G_{p2}} \tag{28}$$

3) Remark: (24) and (28) indicate that $-\frac{\Delta P}{\Delta\omega}$ is a transfer function but not a scalar. The implication is that a given $\Delta\omega$ would lead to two components in ΔP, which are

$$\begin{aligned} \Delta P &= \Delta P_1 + \Delta P_2 \\ \Delta P_1 &= M_{eq} s\Delta\omega; \Delta P_2 = D_{eq}\Delta\omega \end{aligned} \tag{29}$$

where M_{eq} and D_{eq} can be defined as the equivalent inertia and damping coefficient to support the system frequency stability, respectively. Equation (29) indeed underpins the analytical model of DFIG WTs in Fig. 3. When ignoring the dynamics in G_{p1}/G_{p2} (i.e., G_{p1}/G_{p2} is a scalar), M_{eq} and D_{eq} are in proportional to the D-frequency control gain K_d and the P-frequency control gain K_p, respectively. However, the dynamics of G_{p1}/G_{p2} render M_{eq} and D_{eq} a more complicated relationship in respect to different K_d and K_p settings. A detailed explanation will be given in the following section.

V. Impact Mechanism of DFIG WTs on the Ultra-LFO Stability

In this section, the test system in Fig. 3 is adopted to describe the ultra-LFO problem in wind-hydropower systems. The parameters of the HG are given in Section II. A. Revisiting Section III, the inertia M_{eq} and damping coefficient D_{eq} should be calculated by considering two operation modes ($P_0 < 1$pu and $P_0 = 1$pu). They are then used to evaluate DFIG WT's impact on the ultra-LFO stability.

A. Impact Mechanism of DFIG WTs' control on Ultra-LFOs

In this subsection, we consider DFIG WTs working with Scenario A ($P_0 < 1$pu). As it can be seen from Fig. 5, the dynamic behavior of G_{p1} is dependent on the speed control and MPPT control. In combination with the PD-frequency control, they determine the properties of $(-\Delta P/\Delta\omega)$ that is encoded by M_{eq} and D_{eq} in (29). On this basis, three cases are considered to examine how the PD-frequency control, the speed control and MPPT control impact the properties of the inertia M_{eq} and damping D_{eq}.

1) Impact of the PD-frequency control: At first, the speed control is doomed to be sufficiently fast that promises $\Delta\omega_r \approx \Delta\omega_r^{ref}$. M_{eq} and D_{eq} are accordingly dominated by the PD-frequency control settings. (23) and (24) become

$$G_{p1} = a_1/s \tag{30}$$

$$-\frac{\Delta P}{\Delta\omega} = (K_d s + K_p)\frac{s}{s + a_1} \tag{31}$$

where $a_1 = i_{d0}/(2H_r\omega_{r0}^2)$. When compared to (29), we have

$$\begin{aligned} M_{eq} &= K_d\frac{\omega_d^2}{\omega_d^2 + a_1^2} + K_p\frac{a_1}{\omega_d^2 + a_1^2} \\ D_{eq} &= K_d\frac{-\omega_d^2 a_1}{\omega_d^2 + a_1^2} + K_p\frac{\omega_d^2}{\omega_d^2 + a_1^2} \end{aligned} \tag{32}$$

It is interest to note that the change of M_{eq} or D_{eq} depends on whether the multiplier of K_p or K_d is positive or negative. For example, a positive multiplier means that M_{eq} or D_{eq} grows with the increase of K_p or K_d. This also applies to the inertia and damping equations obtained afterward.

Thus, (32) claims that

- The presence of D-frequency control causes a positive M_{eq} (enhancing the system inertia) but a negative D_{eq} (deteriorating the system damping). M_{eq} and the absolute value $|D_{eq}|$ have larger values in the high-frequency range (or with large ω_d).
- With the inclusion of P-frequency control, M_{eq} and D_{eq} are both positive. M_{eq} decreases but D_{eq} increases in the high-frequency range .

2) Impact of the speed control: Then, we consider a relatively slow speed control but the MPPT control time constant T_p is too large to make $\Delta\omega_r^{ref} = 0$. (23) and (24) become

$$G_{p1} = (a_2 + b_2/s)(1/s) \tag{33}$$

$$-\frac{\Delta P}{\Delta\omega} = (K_d s + K_p)\frac{s^2}{s^2 + a_2 s + b_2} \tag{34}$$

The second term of the right side of (34) has the characteristics of a second-order high-pass filter. It is intuitive that the additional frequency control could provide an effective inertia and damping support for the ultra-LFOs when selecting a slow-action speed control (where ($k_{p\omega}$, $k_{i\omega}$) are small, so are (a_2, b_2)). Comparing (29) and (34) yields

$$\begin{aligned} M_{eq} &= \frac{-K_d\omega_d^2(-\omega_d^2 + b_2)}{(-\omega_d^2 + b_2)^2 + (\omega_d a_2)^2} + \frac{K_p\omega_d^2 a_2}{(-\omega_d^2 + b_2)^2 + (\omega_d a_2)^2} \\ D_{eq} &= \frac{-K_d\omega_d^4 a_2}{(-\omega_d^2 + b_2)^2 + (\omega_d a_2)^2} + \frac{-K_p\omega_d^2(-\omega_d^2 + b_2)}{(-\omega_d^2 + b_2)^2 + (\omega_d a_2)^2} \end{aligned} \tag{35}$$

In practice, the speed control is designed by complying with two objectives, including (i) to fast track the speed reference (with requiring a large $k_{i\omega}/k_{p\omega}$,) and (ii) to prevent the mechanical system from excessive transient loads (with requiring a large $k_{p\omega}$ but a small $k_{i\omega}$) [26]. Since the two control objectives are inherently in contradiction, a trade-off should be made between them. Selecting the parameters ($(k_{p\omega}, k_{i\omega}) = (3, 0.6)$) provided in [25] as the basis, some important findings are obtained from (35), as tabulated in

Table I. Note that "↑" represents "increase" and "↓" represents "decrease"; "(+)" and "(−)" represent a positive and a negative sign of the variable, respectively; "abs" represents the absolute value. It can be concluded that (i) the introduction

Table I
M_{eq} AND D_{eq} VARYING WITH SPEED CONTROL PARAMETERS

Precondition		D-frequency control		P-frequency control	
-	-	M_{eq}	D_{eq}	M_{eq}	D_{eq}
-	$k_{p\omega}$,↑	(+),↓	(−),abs↓	(+),↓	(+),↓
$-\omega_d^2+b_2<0$	$k_{i\omega}$,↑	(+),↓	(−),abs↑	(+),↑	(+),↓
$-\omega_d^2+b_2>0$	$k_{i\omega}$,↑	(−),abs↑	(−),abs↓	(+),↓	(−),abs↑
-	T_p,↑	(+),↑	(−),abs↑	(+),↑	(+),↑

of D-frequency control usually causes a negative damping on the ultra-LFO mode, and this phenomenon is even worse for a relatively large $k_{i\omega}$ (where M_{eq} and D_{eq} are both negative); (ii) the P-frequency control is able to produce a well-damped ultra-LFO mode under the case of small $(k_{p\omega}, k_{i\omega})$, since the inertia M_{eq} and the damping D_{eq} are both enhanced (a large M_{eq} further drags the ultra-LFO mode to the low-frequency range). Therefore, a slow-action speed control is useful to conserve the ultra-LFO stability.

3) Impact of the MPPT control: The three feedback loops in G_{p1} are all considered. Revisiting (34), the relationship described by (23) and (24) can be written as

$$G_{p1} = (a_3 + b_3/s)(1/s) \tag{36}$$

$$-\frac{\Delta P}{\Delta\omega} = (K_d s + K_p)\frac{s^2}{s^2 + a_3 s + b_3} \tag{37}$$

associated to the notations

$$a_3 = a_2 + \frac{h_1\omega_{r0}(k_{p\omega}T_p\omega_d^2 + k_{i\omega})}{1 + T_p^2\omega_d^2}$$
$$b_3 = b_2 - \frac{\omega_d^2 h_1\omega_{r0}(k_{p\omega} - k_{i\omega}T_p)}{1 + T_p^2\omega_d^2}$$

[17] states that the speed reference slowly tracks the changes in power with a relatively large T_p. T_p is set at 5 in the WT demo of Matlab/Simulink [25]. If T_p (>5) further increases, a_3 would decrease while b_3 increases first and then decreases, as shown in Fig. 7 (Note that a_3 increases first and then decreases when $T_p<5$). In addition, the presence of T_p makes a_3 and b_3 large than a_2 and b_2, respectively. However, if T_p is large enough, it gives $a_3 \approx a_2$, $b_3 \approx b_2$ and (37) is doomed to be the same as (34). Likewise, the inertia M_{eq} and the

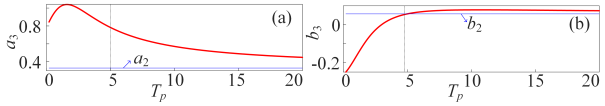

Figure 7. Values of a_3 and b_3 varying with T_p.

damping D_{eq} are formulated as

$$M_{eq} = \frac{-K_d\omega_d^2(-\omega_d^2+b_3)}{(-\omega_d^2+b_3)^2+(\omega_d a_3)^2} + \frac{K_p\omega_d^2 a_3}{(-\omega_d^2+b_3)^2+(\omega_d a_3)^2}$$
$$D_{eq} = \frac{-K_d\omega_d^4 a_3}{(-\omega_d^2+b_3)^2+(\omega_d a_3)^2} + \frac{-K_p\omega_d^2(-\omega_d^2+b_3)}{(-\omega_d^2+b_3)^2+(\omega_d a_3)^2} \tag{38}$$

Consider that $(k_{p\omega}, k_{i\omega}) = (3, 0.6)$ and T_p is initially set at 5. Table I presents the properties of M_{eq} and D_{eq} varying with further increasing T_p (>5, and $-\omega_d^2+b_3<0$ from Fig. 7). It is acknowledged that (i) when D-frequency control engages, a smaller T_p is preferred due to introducing a reduced negative damping; however, (ii) when P-frequency control engages, a larger T_p is preferred since M_{eq} and D_{eq} are both enhanced.

B. Consideration of the Impact of Operation Mode

It is known that the control of DFIG WTs have different behaviors under different operation modes. In this segment, we explore the mechanism of DFIG WTs involved in the ultra-LFO problems under Scenario B-$P_0 = 1$pu. The MPPT control output is clamped to make $\omega_r^{ref} = 1.2$pu; the speed control is the same compared to the case of $P_0 < 1$pu. To avoid overlapping work, the foremost concern is then toward investigating the impacts of the (ω_r-regulated) pitch control and pitch compensation control on the frequency-responsive DFIG WT's behaviors at the ultra-LFO mode.

1) The impact of the ω_r-regulated pitch control: To give a straightforward analysis, we discard the impact of pitch compensation control herein. (27) becomes

$$G_{p2} = (a_2 + b_2/s)(1/(s + k'_{p\beta1})) \tag{39}$$

The second term of the right-side (36) functions as a low-filter pass with the time constant in proportional to the parameter $k_{p\beta1}$. The presence of $k'_{p\beta1}$ makes G_{p2} in (39) have a phase boost compared to G_{p1} in (33), thus producing an enhanced effectiveness of the speed control in stabilizing the ultra-LFOs (that exist in the rotor speed/electrical power).

According to (39), (28) becomes

$$-\frac{\Delta P}{\Delta\omega} = (K_d s + K_p)\frac{s^2 + k'_{p\beta1}s}{s^2 + (a_2 + k'_{p\beta1})s + b_2} \tag{40}$$

Compared to (29), M_{eq} and D_{eq} can be obtained

$$\begin{aligned} M_{eq} &= \omega_d^2 K_d \frac{k'_{p\beta1}(k'_{p\beta1}+a_2) - (-\omega_d^2+b_2)}{(-\omega_d^2+b_2)^2 + (\omega_d k'_{p\beta1}a_2)^2\omega_d^2} \\ &\quad + K_p \frac{\omega_d^2(a_2+k'_{p\beta1}) + k'_{p\beta1}(-\omega_d^2+b_2)}{(-\omega_d^2+b_2)^2 + (\omega_d k'_{p\beta1}a_2)^2\omega_d^2} \\ D_{eq} &= -\omega_d^2 K_d \frac{(a_2+k'_{p\beta1}) + k'_{p\beta1}(-\omega_d^2+b_2)}{(-\omega_d^2+b_2)^2 + (\omega_d k'_{p\beta1}a_2)^2\omega_d^2} \\ &\quad + \omega_d^2 K_p \frac{k'_{p\beta1}(k'_{p\beta1}+a_2) - (-\omega_d^2+b_2)}{(-\omega_d^2+b_2)^2 + (\omega_d k'_{p\beta1}a_2)^2\omega_d^2} \end{aligned} \tag{41}$$

Using the parameters given by [25], the presence of $k'_{p\beta1}$ causes a positive M_{eq} but a negative D_{eq} under the case of D-frequency control, while M_{eq} and D_{eq} are both positive under the case of P-frequency control. While $(-\omega_d^2+b_2)$ is small enough and omitted relative to $(a_2+k'_{p\beta1})$, the absolute M_{eq} and D_{eq} are around opposite to $k'_{p\beta1}$ (see Table II).

2) The impact of the pitch compensation control: Contemplating the impact of pitch compensation control, (27) becomes

$$G_{p2} = (a_2 + b_2/s)(k'_{p\beta} + k'_{i\beta}/s) \tag{42}$$

The second term of the right-side (42) is associated with the pitch compensation control. It equivalently provides a

PI-type control (with a lagged phase) supplemented to the speed control, reducing the speed control margin. That is, the pitch compensation control deteriorates the effectiveness of the speed control in hindering the ultra-LFOs. (42) is rewritten as

$$G_{p2} = (a_4 + b_4/s)(1/s) \tag{43}$$

where $a_4 = a_2 k'_{i\beta} + b_2 k'_{p\beta}$, $b_4 = -\omega_d^2 a_2 k'_{p\beta} + b_2 k'_{i\beta}$. Thus, (25) becomes

$$-\frac{\Delta P}{\Delta \omega} = (K_d s + K_p)\frac{s^2}{s^2 + a_4 s + b_4} \tag{44}$$

Along with (22), M_{eq} and D_{eq} are formulated as

$$\begin{aligned} M_{eq} &= \frac{-K_d\omega_d^2(-\omega_d^2 + b_4)}{(-\omega_d^2 + b_4)^2 + (\omega_d a_4)^2} + \frac{K_p\omega_d^2 a_4}{(-\omega_d^2 + b_4)^2 + (\omega_d a_4)^2} \\ D_{eq} &= \frac{-K_d\omega_d^4 a_4}{(-\omega_d^2 + b_4)^2 + (\omega_d a_4)^2} + \frac{-K_p\omega_d^2(-\omega_d^2 + b_4)}{(-\omega_d^2 + b_4)^2 + (\omega_d a_4)^2} \end{aligned} \tag{45}$$

In accordance to [17] and [25], $k_{p\beta}$ is relatively small and $k_{p\beta} \ll k_{i\beta}$ to comply with the pitch angle regulation and stability requirements. When considering an increase of $k_{i\beta}$, a_4 and b_4 both increase. Likewise, the properties of M_{eq} and D_{eq} can be obtained and presented in Table II.

Table II
M_{eq} AND D_{eq} VARYING WITH PITCH CONTROL SETTINGS

Precondition	D-frequency control		P-frequency control	
-	M_{eq}	D_{eq}	M_{eq}	D_{eq}
$k_{p\beta 1}$,↑	(+),↓	(−),abs↓	(+),↓	(+),↓
$k_{i\beta}$,↑	(−),abs↑	(−),abs↓	(+),↓	(−),abs↑

C. Validation of the Analysis Results

In this subsection, the linearized analytical model and the detailed time-domain model of the 2-machine test system are established in Matlab/Simulink to validate the aforementioned analysis results.

1) Modal analysis results: The modal analysis is carried out to better comprehend the mechanisms of the ultra-LFO mode eigenvalues changing with the DFIG WT behaviors. The scenarios of DFIG WT operating with $P_0 < 1$pu and $P_0 = 1$pu are both considered. Without the PD-frequency control, the critical eigenvalues $\lambda_{1,2} = 0.0068 \pm j0.374$ under $P_0 < 1$pu or $\lambda_{1,2} = 0.0095 \pm j0.377$ under $P_0 = 1$pu. This implies an unstable ultra-LFO mode that oscillates at around 0.06Hz. The participation factors (PFs) of DFIG WT's control in the ultra-LFO mode are presented in Table III.

Table III
PARTICIPATION FACTOR OF WT CONTROL IN THE ULTRA-LFO MODE

Precondition		D control	P control	Speed control	MPPT control	$k_{p\beta 1}$ control	Pitch com- control
K_d, $K_p = 0$	-	-	-	≈ 0	≈ 0	≈ 0	≈ 0
$K_d = 20$	$P_0 < 1$	0.018+j0.037	-	0.013+j0.014	-0.002-j0.0043	-	-
$K_p = 0$	$P_0 = 1$	0.097+j0.041	-	0.042-j0.012	-	-0.0001-j0.0004	0.093+j0.066
$K_d = 0$	$P_0 < 1$	-	-0.001-j0.0073	0.015-j0.13	-0.004+j0.0013	-	-
$K_p = 10$	$P_0 = 1$	-	0.0001-j0.0048	0.017-j0.066	-	-0.0003-j0.0004	0.14-j0.055

The critical eigenvalues have a left shift $\Delta\lambda_{1,2}$ based on the control-gain change Δk and the corresponding PF [27]

$$\Delta\lambda_{1,2} = -\left\{PF_R(\lambda_{1,2}) + jPF_I(\lambda_{1,2})\right\}\Delta k \tag{46}$$

where $PF_R(\lambda_{1,2})$ and $PF_I(\lambda_{1,2})$ denote the real and imaginary part of the concerned PF corresponding to the ultra-LFO mode. Supposing an increase of the control gain, $\lambda_{1,2}$ would shift left for $PF_R(\lambda_{1,2}) < 0$ and move down for $PF_I(\lambda_{1,2}) < 0$. Accordingly, the following findings can be concluded from Table III.

- Without the frequency control, the ultra-LFO mode stability is dictated by HG's inertia, governor control and turbine behavior, but hardly relevant to DFIG WT control.
- The introduction of D-frequency control has a positive PF_R and thus provokes DFIG WT to create an adverse impact on the ultra-LFO mode stability.
- The P-frequency control enables a negative PF and hence a positive damping on the ultra-LFO mode stability.
- By creating a positive PF_R, a slow speed control (small ($k_{p\omega}$, $k_{i\omega}$)) could enhance the ultra-LFO stability.
- The MPPT control fitted with a small time constant T_p helps resume the ultra-LFO stability.
- Under $P_0 = 1$pu, the ω_r regulated pitch control allows an improved damping on the ultra-LFO, while the pitch angle compensation control (having a positive PF_R) imposes an adverse impact on the ultra-LFO mode.

Although the PF of DFIG WT's control in the ultra-LFO mode is sometimes small, these control parameters generally have large values (in compliance with their original design requirements [17]) and still reinforce a considerable impact on the ultra-LFO stability. This can be more visually observed in the following time-domain results.

2) Time-domain simulation results: The time-domain model has been augmented with the models presented in [25]. The key parameters of the HG and DFIG WT are referred to Appendix. The DFIG WT operates at 10m/s, and the instantaneous penetration of wind power achieves 60.56% in the steady state. In what follows, the test system confronts with a step increment of the load at $t = 1s$. Fig. 8-Fig. 11 shows the simulation results by considering DFIG WTs under different control implementations and operation modes.

As it can be seen from Fig. 8, we have that

- When the D-frequency control engages, the system speed swings with a smaller ultra-LFO mode frequency (see 8 (a)). This is because that the D-frequency controlled DFIG WT provides an enhanced inertia support (positively related to K_d), which drags the ultra-LFO to the low-frequency range where the 2-machine system has an improved damping. The first-swing stability is improved meanwhile. Notably, the subsequent swings (with the time evolution) suffer from an increased overshoot (even a serious instability phenomenon observed in Fig. 13).
- When the P-frequency control engages, the frequency collapse is avoided and the frequency nadir is lifted (see 8 (b)). In addition, the increase of K_p enables the system frequency to be more easily stabilized and better-damped. This is because that the DFIG WTs provide a substantial damping support on the ultra-LFO mode, especially for a large K_p.
- The PD-frequency control produces the best frequency response since it enhances both the system inertia and

the damping (see 8 (c)). The PD-frequency control not only drags the ultra-LFO mode frequency to the low-frequency range, but also well damps the ultra-LFO. This suggests to make a trade-off between the inertia and stability requirements when selecting the PD-frequency control implementation.

Fig. 9 shows the impact of speed control on the system frequency. (i) When the D-frequency control engages, the ultra-LFO mode frequency and the overshoot are both reduced with a slow-action speed control ($k_{i\omega}/k_{p\omega}$ kept constant). (ii) When the P-frequency control engages, the ultra-LFO mode could be stabilized and well-damped through deploying a slower-action speed control. As the displayed by Fig. 9, the purple line presents a best frequency response under each case. Thus, in case of a slow-action speed control, the frequency-responsive DFIG WT is able to drastically mitigate the ultra-LFO problem since the inertia and damping are both enhanced.

Fig. 10 shows the impact of the MPPT control on the system frequency. (i) When the D-frequency control engages, the ultra-LFO mode frequency and overshoot are both reduced with a smaller T_p (see Fig. 10 (a)). This is because of a smaller negative damping from the DFIG WT in this case. (ii) When the P-frequency control engages, a large T_p is suggested to damp the ultra-LFO mode (see Fig. 10 (b)). This is because that increasing T_p enables the DFIG WT to provide an enhanced inertia and damping support.

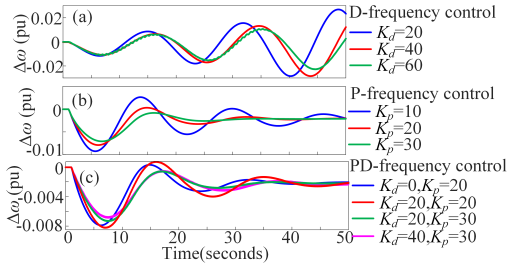

Figure 8. Responses of the frequency-responsive DFIG WT under different PD-frequency control settings ($P_0 = 0.54$pu).

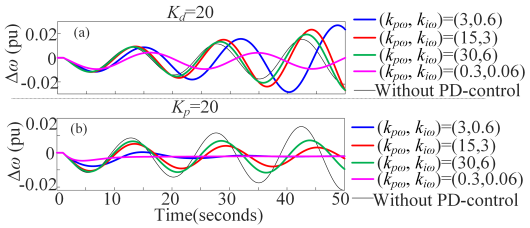

Figure 9. Responses of the frequency-responsive DFIG WT under different speed control settings ($P_0 = 0.54$pu).

In Fig. 11, four different pitch control settings are considered under the case of the D-frequency or P-frequency control installed. Under each case, the absence of the ω_r-regulated pitch control causes a worst ultra-LFO stability (displayed by the purple line). By reducing the impact of the pitch compensation control, the ultra-LFO stability can be improved (comparing the responses denoted by the blue and red lines). Thus, the results demonstrate that

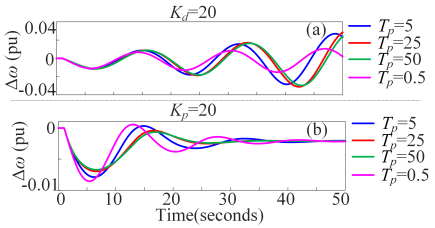

Figure 10. Responses of the frequency-responsive DFIG WT under different MPPT time constants ($P_0 = 0.54$pu).

- The ω_r-regulated pitch control assists to damp the ultra-LFO mode. Note that when the P-frequency control engages, the ultra-LFO mode frequency and the overshoot both increase with the increasing of $k_{p\beta 1}$ since the inertia and damping support are both reduced.
- The pitch compensation control drastically deteriorates the ultra-LFO mode and causes a more serious system speed collapse. The collapse appears at the consequence that the pitch compensation control causes the PD-frequency controlled DFIG WT to impose a negative damping effect on the ultra-LFO mode.

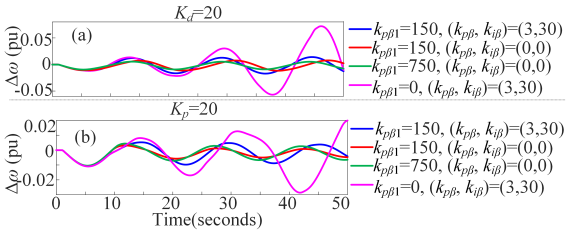

Figure 11. Responses of the frequency-responsive DFIG WT under different pitch control settings ($P_0 = 1.0$pu).

VI. Simulation Study

In this section, we extend the analysis to a modified 10-machine 39-bus New-England power system shown in Fig. 12 [28]. For convenience, it has been divided into 3 areas, wherein the steam-turbine generators SG1-SG7 in Area II and III are replaced by six HGs (including HG1-HG6) and a DFIG WT. The data of SG8-SG10, lines and loads are referred to [28]. Each HG is rated at 1000 MVA. The HYGOV settings are: $R_p = 0.05$, $T_G = 0.2$, $T_w = 1$, $T_R = 5$, $R_T = 0.38$, $M = 2H = 13$ and $D = 0$ [21]. The DFIG WT is aggregated by 600 1.5-MW GE WTs and totally rated at 900 MW. Other key parameters of the HG and DFIG WT are referred to [25].

At first, the DFIG WT operates under 10m/s and the frequency control is disabled. When a step increment of the load occurs at Bus 24 at $t = 1$ s, the system speed is under-damped with an oscillation frequency at around 0.0714Hz. Then, we tend to closely study the impact of frequency-responsive DFIG WTs (fitted with a PD-frequency control) on the ultra-LFO mode under different control settings and operation modes. With each type of frequency control implementation, three cases are examined to show the impact of WT's behaviors on the ultra-LFO stability. Total 24 cases have been studied and listed in Table IV. Note that (i) in Case 7-Case 24, $K_d = 40$

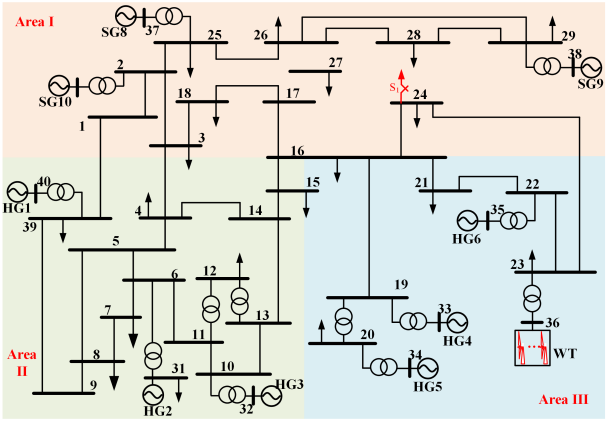

Figure 12. One-line diagram of the modified 10-machine 39-bus test system.

for D-frequency control and $K_p = 20$ for P-frequency control; (ii) other parameters remain the same as [25], if without specifically mentioned.

Table IV
CASE STUDY SETTINGS

Case 1-3 (D-control)	$K_d = 20$	$K_d = 40$	$K_d = 80$
Case 4-6 (P-control)	$K_p = 10$	$K_p = 20$	$K_p = 30$
Case 7-9 (D-control)	$k_{p\omega} = 15$	$k_{p\omega} = 30$	$k_{p\omega} = 0.3$
Case 10-12 (P-control)	$k_{i\omega} = 3$	$k_{i\omega} = 6$	$k_{i\omega} = 0.06$
Case 13-15 (D-control)	$T_p = 25$	$T_p = 50$	$T_p = 0.5$
Case 16-18 (P-control)			
Case 19-21 (D-control)	$k_{p\beta 1} = 0$	$k_{p\beta 1} = 150$	$k_{p\beta 1} = 750$
Case 22-24 (P-control)	$(k_{p\beta}, k_{i\beta}) = (3, 30)$	$(k_{p\beta}, k_{i\beta}) = (0, 0)$	$(k_{p\beta}, k_{i\beta}) = (0, 0)$

The simulation results are presented in Fig. 13-Fig. 16, where we can make several insightful observations that validate the analysis results raised in Section IV. Fig. 13 is obtained by considering the impact of PD-frequency control parameters. (i) With the increase of K_d, the first-swing stability is enhanced but the system frequency would be in danger of collapse for a relatively large K_d (i.e., 80). (ii) By increasing the gain K_p, the ultra-LFO can be better damped and the system frequency reaches the steady state in a shorter time. Thus, (i) the D-frequency control enhances the system inertia but imposes an adverse impact on the ultra-LFO mode; in contrast, (ii) the P-frequency control empowers the system to well damp the ultra-LFO mode.

In Fig. 14, the impact of the speed control is considered. Under the case of D-frequency or P-frequency control, the ultra-LFO is always mitigated if $(k_{p\omega}, k_{i\omega})$ are selected with small values (displayed by the purple lines). This demonstrates that a slow-action speed control (with small $(k_{p\omega}, k_{i\omega})$) makes the DFIG WT and the system become significantly less prone to ultra-LFO issues.

In terms of MPPT, it can be cast as a supplemented proportional speed feedback with a low-pass filter before going through the speed control. The time constant T_p is usually large. Fig. 15 claims that a large T_p further enhances the ultra-LFO damping from the P-frequency controlled DFIG WT, while a small T_p is advantageous for the D-frequency controlled DFIG WT.

Finally, we pay attention to the notion that DFIG WT's pitch control would have a considerable participation in the ultra-LFO dynamic during the rated-power operation. Fig. 16 showcases that (i) the system frequency collapse is more serious when sacrificing the the ω_r-regulated pitch control (displayed by the purple line); (ii) the ultra-LFO stability is slightly improved by reducing the impact of pitch compensation control. Thus, it proves that (i) the ω_r-regulated pitch control is beneficial to helping conserve the ultra-LFO stability (with significantly reducing the overshoot); (ii) the pitch compensation control imposes an adverse impact on the ultra-LFO stability (since it causes the system speed diverging at the ultra-LFO mode). Therefore, it is recommended that

- The P-frequency control is required for empowering DFIG WTs to support the ultra-LFO stability.
- The D-frequency control is deployed in compliance with the system inertia requirement. A trade-off should be made between the inertia support and the damping support to conserve and optimize the dynamic stability of a wind-hydropower hybrid system.
- A slow-action speed control allows frequency-responsive DFIG WTs to provide a better damping support on the ultra-LFO mode.
- Under the rated-power operation, the ω_r-regulated pitch control is needed to counteract the ultra-LFO damping degradation caused by the pitch compensation control.

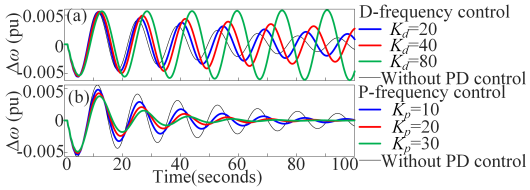

Figure 13. System speed of frequency-responsive DFIG WTs ($P_0 = 0.54$pu) under different K_d and K_p values.

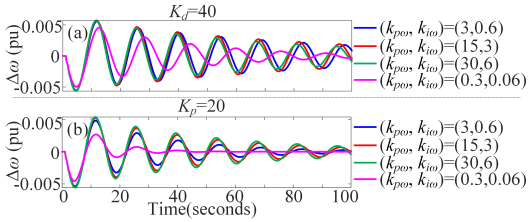

Figure 14. System speed of frequency-responsive DFIG WTs ($P_0 = 0.54$pu) under different speed control settings.

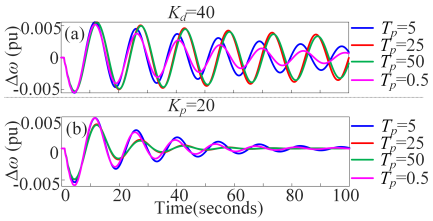

Figure 15. System speed of frequency-responsive DFIG WTs ($P_0 = 0.54$pu) under different MPPT time constants.

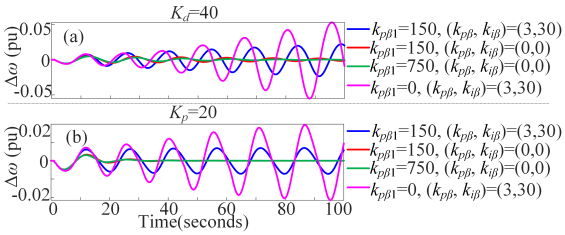

Figure 16. System speed of frequency-responsive DFIG WTs (P_0 = 1pu) under different pitch control settings.

VII. Conclusions

This paper carries out an examination on the behaviors of DFIG WTs participating in the power system ultra-LFOs, through an analytical model and a torque analysis method. In this course, we calculate the inertia and damping support from DFIG WTs, and examine the ultra-LFO stability subject to WTs' primary control settings. The analytical study is performed on a 2-machine hybrid system. In addition, a more rigorous result validation is carried out using a modified 10-machine 39-bus New-England power system.

This paper shows the following. (i) DFIG WTs offer a considerable inertia and damping support to the ultra-LFO mode through the PD-frequency control. (ii) The D-frequency control gain dictates the inertia support. Although it resists the first-swing stability of the ultra-LFO, the ultra-LFO instability phenomena may appear with an undue increase of the control gain (K_d). (iii) The P-frequency control allows DFIG WTs to rescue the ultra-LFO stability. The damping support reinforces with the increase of control gain (K_p). (iv) The speed control functions as a second-order high-pass filter seen from the relationship of $(-\Delta P/\Delta\omega)$. It allows a slow-action speed control to rescue the ultra-LFO stability. (v) Under the rated-power operation, the ω_r-regulated pitch control does have a positive impact but the pitch compensation control imposes a negative impact on the ultra-LFO mode. (vi) We therefore conclude that the DFIG WT provides better controllability to mitigate ultra-LFOs by modifying its control configuration, subject to a trade-off between the inertia and damping requirements.

Appendix

Table V lists some reported papers associated to modeling WTs for power system dynamic stability.

Table V
Models for WTs involved in power system dynamic stability

	Objective	Focused time scale	Focused controls and dynamics	Notes
Model in [12], [13]	Inertial response study	0.1-2s	Generator dynamics, speed control, (slow-action) PLL control	Discarding the fast dynamics (DC-link, DC/AC voltage control), and the slow dynamics (MPPT/pitch control)
Model in [11]	Torsional oscillation study	0.05-0.1s	Generator dynamics, speed control, PD-frequency control	
Model in [19]	Electromechanical oscillation (focus on LFO) study	0.1-3s	Generator dynamics, speed control, DC-link dynamics, DC/AC-voltage control, frequency control	Discarding the slow dynamics (MPPT/pitch control)
Model in [14], [15]	Subsynchronous oscillation study	0.01-0.1s	DC-link dynamics, DC/AC-voltage control, line dynamics, capacitor dynamics	Discarding generator dynamics, speed control and the slow dynamics (MPPT/pitch control)

References

[1] I. Kamwa, D. Lefebvre, and L. Loud, "Small signal analysis of hydro-turbine governors in large interconnected power plants," in *Proc. IEEE Power Eng. Soc. Winter Meeting*, vol. 2, pp. 1178-1183, 2002.

[2] H. V. Pico, J. D. McCalley, A. Angel, R. Leon, and N. J. Castrillon, "Analysis of very low frequency oscillations in hydro-dominant power systems using multi-unit modeling," *IEEE Trans. Power Syst.*, vol. 27, no. 4, pp. 1906-1915, Nov. 2012.

[3] W. Mo, Y. Chen, H. Chen, Y. Liu, Y. Zhang, J. Hou, and C. Li, "Analysis and measures of ultralow-frequency oscillations in a large-scale hydropower transmission system," *IEEE Journal of Emerging and Selected Topics in Power Electronics*, vol. 6, no. 3, pp. 1077-1085, 2017.

[4] E. B. Shahrodi, A. Norched, "Dynamic behaviour of AGC systems including the effects of nonlinearities," *IEEE Trans. Power App. Syst.*, vol. PAS-104, no. 12, pp. 3409-3415, 1985.

[5] L. Chen, X. Lu, Y. Min, Y. Zhang, Q. Chen, Y. Zhao, and C. Ben, "Optimization of governor parameters to prevent frequency oscillations in power systems," *IEEE Trans. Power Syst.*, vol. 33, no. 4, pp. 4466-4474, July 2018.

[6] Canwea, "Wind energy in Qubec," News, Dec. 2019, [Online]. Available: https://canwea.ca/wind-energy/quebec/

[7] E. N. Hinrichsen, and P. J. Nolan, "Dynamics and stability of wind turbine generators," *IEEE Power Eng. Rev.*, vol. PER-2, no. 8, pp. 38-39, Aug. 1982.

[8] National Code, "The Grid Code (Issue 5)," Mar. 2017. [Online]. Available: https://www.nationalgrideso.com/document/34101/download

[9] Hydro-Qubec Transnergie, "Technical requirements for the connection of generating stations to the Hydro-Qubec transmission system," Technical Report, Jan. 2019.

[10] Y. Mishra, S. Mishra, F. Li, Z. Y. Dong, and R. C. Bansal, "Small-signal stability analysis of a DFIG-based wind power system under different modes of operation," *IEEE Trans. Energy Convers.*, vol. 24, no. 4, pp. 972-982, Dec. 2009.

[11] M. F. Arani, and Y. A. R. I. Mohamed, "Analysis and damping of mechanical resonance of wind power generators contributing to frequency regulation," *IEEE Trans. Power Syst*, vol. 32, no. 4, pp. 3195-3204, 2017.

[12] M. F. Arani, and Y. A. R. I. Mohamed, "Implementing virtual inertia in DFIG-based wind power generation," *IEEE Trans. Power Syst*, vol. 28, no. 2, pp. 1373-1384, May 2013.

[13] W. He, X. Yuan, and J. Hu, "Inertia provision and estimation of PLL-based DFIG wind turbines," *IEEE Trans. Power Syst.*, vol. 32, no. 1, pp. 510-521, Jan. 2017.

[14] L. Fan, R. Kavasseri, Z. L. Miao, and C. Zhu, C, "Modeling of DFIG-based wind farms for SSR analysis," *IEEE Trans. Power Deliv.*, vol. 25, no. 3, pp. 2073-2082, Oct. 2010.

[15] W. Du, C. Chen, and H. Wang, "Subsynchronous interactions induced by DFIGs in power systems without series compensated lines," *IEEE Trans. Sustain. Energy*, vol. 9, no. 3, pp. 1275-1284, July 2018.

[16] D. Bourlis, and R. Carriveau, "A complete control scheme for variable speed stall regulated wind turbines," Fundamental and advanced topics in wind power, pp. 309-339, July 2011.

[17] K. Clark, N. W. Miller, and J. J. Sanchez-Gasca, "Modeling of GE wind turbine-generators for grid studies," GE Inc., Schenectady, NY, Tech. Rep. Version 4.5, Apr. 2010.

[18] M. Niasse, Q. Zheng, A. Xin, F. A. F. Quan, "Mitigating ultra-low-frequency oscillations in wind-penetrated hydro-dominant power grid through virtual inertia emulation strategy," In *2020 4th International Conference on Power and Energy Engineering (ICPEE), IEEE*, 2020.

[19] W. Du, X. Chen and H. F. Wang, "Impact of dynamic interactions introduced by the DFIGs on power system electromechanical oscillation modes," *IEEE Trans. Power Syst.*, vol. 32, no. 6, pp. 4954-4967, Nov. 2017.

[20] L. Sun, K. Liu, J. Hu, and Y. Hou, "Analysis and mitigation of electromechanical oscillations for DFIG wind turbines involved in fast frequency response," *IEEE Trans. Power Syst.*, vol. 34, no. 6, pp. 4547-4556, Nov. 2019.

[21] P. Kundur, *Power system stability and control*, New York: McGraw-Hill, 1994.

[22] R. Farmer, "Power systems dynamics and stability," in *The Electric Power Engineering Handbook*, L. Grigsby, Ed. Boca Raton, FL: CRC, 2001.

[23] R. Xie, Ruichao, I. Kamwa, D. Rimorov, and A. Moeini, "Fundamental study of common mode small-signal frequency oscillations in power systems," *International Journal of Electrical Power & Energy Systems*, 106, pp. 201-209, Mar. 2019.

[24] G. Chen, F. Tang, H. Shi, R. Yu, G. Wang, L. Ding, and X. Lu, "Optimization strategy of hydrogovernors for eliminating ultralow-frequency oscillations in hydrodominant power systems," *IEEE Journal of Emerging and Selected Topics in Power Electronics*, vol. 6, no. 3, pp. 1086-1094, Sept. 2018.
[25] The MathWorks, "Wind farm-DFIG average model," and "29-bus, 7-power plant network model," Sept. 2018. [Online]. Available: https://mathworks.com
[26] F. D. Bianchi, H. De Battista, and R. J. Mantz, *Wind turbine control systems: Principles, modelling and gain scheduling design*. Springer Science & Business Media, Sept. 2006.
[27] M. J. Gibbard, P. Pourbeik, and D. J. Vowles, *Small-signal stability, control and dynamic performance of power systems*, University of Adelaide press, 2015.
[28] M. A. Pai, *Energy function analysis for power system stability*. Springer Science & Business Media, 2012.

Li Sun received the B. Eng. degree and the M.Eng. degrees from Huazhong University of Science and Technology (HUST), Wuhan, China, in 2013, and 2016 respectively, and the Ph.D. degree from The University of Hong Kong, Hong Kong, in 2019, both in electrical engineering. After that she worked as a Research Fellow with the University of Warwick, United Kingdom until June 2021. She is currently an Assistant Professor with the School of Mechanical Engineering and Automation, Harbin Institute of Technology, Shenzhen. Her current research interests focus on the power system stability control, control design and optimization of islanded microgrids.

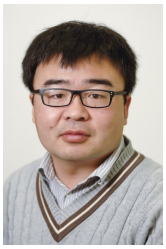

Xiaowei Zhao is Professor of Control Engineering and an EPSRC Fellow at the School of Engineering, University of Warwick, Coventry, UK. He obtained the PhD degree in Control Theory from Imperial College London in 2010. After that he worked as a postdoctoral researcher at the University of Oxford for three years before joining Warwick in 2013. His main research areas are control theory with applications on offshore renewable energy systems, local smart energy systems, and autonomous systems.